Electrochemical Behavior of Magnetron-Sputtered Al-Cu Alloy Films in Sulfate Solutions

Jonathan Idrac, Christine Blanc, Yolande Kihn, Marie-Christine Lafont, Georges Mankowski, Peter Skeldon, George Thompson

▶ **To cite this version:**

Jonathan Idrac, Christine Blanc, Yolande Kihn, Marie-Christine Lafont, Georges Mankowski, et al.. Electrochemical Behavior of Magnetron-Sputtered Al-Cu Alloy Films in Sulfate Solutions. Journal of The Electrochemical Society, 2007, vol. 154, pp.C286-C293. 10.1149/1.2719623 . hal-00806052

HAL Id: hal-00806052
https://hal.science/hal-00806052

Submitted on 29 Mar 2013

HAL is a multi-disciplinary open access archive for the deposit and dissemination of scientific research documents, whether they are published or not. The documents may come from teaching and research institutions in France or abroad, or from public or private research centers.

L'archive ouverte pluridisciplinaire **HAL**, est destinée au dépôt et à la diffusion de documents scientifiques de niveau recherche, publiés ou non, émanant des établissements d'enseignement et de recherche français ou étrangers, des laboratoires publics ou privés.

Open Archive Toulouse Archive Ouverte (OATAO)
OATAO is an open access repository that collects the work of Toulouse researchers and makes it freely available over the web where possible.

This is an author-deposited version published in: http://oatao.univ-toulouse.fr/
Eprints ID : 2425

To link to this article :
URL : http://dx.doi.org/10.1149/1.2719623

To cite this version : Idrac, Jonathan and Blanc, Christine and Kihn, Yolande and Lafont, Marie-Christine and Mankowski, Georges and Skeldon, P. and Thompson, George (2007) *Electrochemical Behavior of Magnetron-Sputtered Al–Cu Alloy Films in Sulfate Solutions.* Journal of The Electrochemical Society (JES), vol. 154 (n° 6). C286-C293. ISSN 0013-4651

Any correspondence concerning this service should be sent to the repository administrator: staff-oatao@inp-toulouse.fr

Electrochemical Behavior of Magnetron-Sputtered Al–Cu Alloy Films in Sulfate Solutions

J. Idrac,[a] Ch. Blanc,[a,*,z] Y. Kihn,[b] M. C. Lafont,[a] G. Mankowski,[a] P. Skeldon,[c,*] and G. E. Thompson[c,]**

[a]*Centre Interuniversitaire de Recherche et d'Ingéniere des Matériaux, UMR CNRS 5085, ENSIACET, 31077 Toulouse Cedex 04, France*
[b]*Centre d'Elaboration des Matériaux et d'Etudes Structurales, UPR 8011, 31055 Toulouse Cedex 04, France*
[c]*Corrosion and Protection Center, School of Materials, The University of Manchester, Manchester M60 1QD, United Kingdom*

Model alloys, generated by magnetron sputtering, have been employed to understand the role of copper on the corrosion behavior of aluminum alloys. Binary Al–Cu alloys, with copper contents between 0 and 100 atom %, were synthesized with well-controlled compositions, embracing single-phase α and θ alloys together with multiphase alloys. Electrochemical measurements confirmed the stability of the thin alloy films and revealed that the corrosion behavior of the α, θ, and η_2 phases differed strongly in the cathodic region. Further, in the anodic region, phases of high copper content suffered pitting in sulfate solutions, while the α phase remained passive.

[DOI: 10.1149/1.2719623]

There is significant interest in the corrosion behavior in aerated solutions of aluminum alloys containing copper, which are of importance in many sectors, including aerospace. In the alloys, copper is present in the matrix and in various fine strengthening phases and coarse constituent particles. In appropriate media, localized corrosion, such as pitting, can occur; galvanic coupling between the matrix and particles also drives alkaline corrosion of the matrix regions adjacent to cathodic sites. The importance of intermetallic particles as initiation sites for corrosion is the subject of wide discussion.[1-3] In order to further examine their role, various electrochemical approaches, for example, impedance spectroscopy, have been used.[4,5] However, as indicated by Schmutz et al., many electrochemical methods lack the lateral resolution, that is necessary for probing the role of micrometer-sized constituent particles in localized corrosion.[6,7] The previous authors used atomic force microscopy (AFM), with in situ scratching and Volta potential mapping, to examine localized corrosion of aluminum alloys. Campestrini et al. also used AFM to identify and to quantify galvanic coupling between the aluminum matrix and Al–Cu–Mg containing particles in an AA2024 alloy.[8] The previous examples show a clear influence of copper-containing intermetallics on the corrosion resistance of aluminum alloys, but mechanisms to explain the dissolution of the intermetallics, the associated copper enrichment, and pit nucleation at these sites remain unclear, despite their extensive study.[2,3,9] In addition, Buccheit et al. stated, "This Cu ion generation mechanism is believed to be a significant factor contributing to the poor corrosion resistance and poor conversion coating characteristics of Al_2CuMg bearing alloys," confirming that appropriate study is needed to understand precisely the performance of these important structural aluminum alloys.[9] Many studies are now employing electrochemical techniques at the micrometer scale; thus, Suter and Alkire studied pitting on AA2024 T3 alloy in a microelectrochemical cell.[10] They showed that Al–Cu–Mg particles were the least corrosion-resistant sites, and before such particles were completely dissolved, pitting started at the adjacent matrix. Other studies using microelectrodes, performed on AA2024 T3 alloy, showed that Al–Cu–Mg particles acted as anodic sites, whereas Al–Cu–Mn–Fe particles were cathodic sites.[11]

In commercial aluminum-copper alloys, the copper content of the particles highly varies depending on the alloy type and the particles. It can also vary during exposure to an aggressive medium because of copper enrichment. Additionally, if the particles contain other alloying elements, such as Mg, Mn, or Fe, copper has the main influence on the electrochemical behavior of the particles due to its high content. Consequently, this paper examines the influence of copper content (varying over a wide range) in binary aluminum-copper alloys on the corrosion behavior.

The alloys, with copper contents up to 100%, were prepared by magnetron sputtering;[12-14] the microstructure was examined by transmission electron microscopy (TEM), associated with energy-dispersive X-ray spectroscopy (EDS), and electron energy loss spectroscopy (EELS). Electron diffraction was also performed to determine the phases present in the alloys and their stability. The electrochemical behavior of the materials was examined using potential-time responses and polarization studies.

Experimental

Material.— Binary Al–Cu alloy films, with copper contents between 0 and 100 atom % copper, were deposited using an Atom Tech, Ltd., magnetron sputtering with separate high-purity aluminum (99.999%) and copper (99.99%) targets. The substrates onto which the alloys were deposited consisted of electropolished 99.99% aluminum foils. The alloy layers were deposited at a rate of about 9 nm min^{-1} to a total thickness in the approximate range 400–500 nm. The deposition chamber was first evacuated to 4×10^{-7} mbar, with sputtering then carried out at 5×10^{-3} mbar in 99.998% argon at 300 K.

TEM examination.— TEM observations of the thin deposits were performed by using a JEOL JEM 2010 microscope operating at 200 kV and equipped with a TRACOR EDS spectrometer. Cross sections of the freshly deposited alloys were prepared. Initially, two thin slices, cut normally to the film/substrate interface with a diamond saw, were prepared. The slices were then glued together, film to film, and embedded in a 3 mm diameter brass tube with a Gatan epoxy resin. After curing, the tube was sectioned into approximately 300 μm disks, which were polished on the exposed faces and dimpled before ion milling to transparency with a PIPS (Gatan) precision ion-polishing system. The PIPS utilizes relatively high-power ion guns (0–6 keV) at a low angle of incidence (0–10°). The cross sections were also observed on a Philips CM20T TEM, operating at 200 kV, and equipped with an electron energy-loss spectrometer, allowing energy loss near edge structures (ELNES) to be acquired for local chemical analysis. Electron diffraction was also undertaken on this microscope, using a beam of fine diameter (<10 nm).

* Electrochemical Society Active Member.
** Electrochemical Society Fellow.
z E-mail: Christine.Blanc@ensiacet.fr

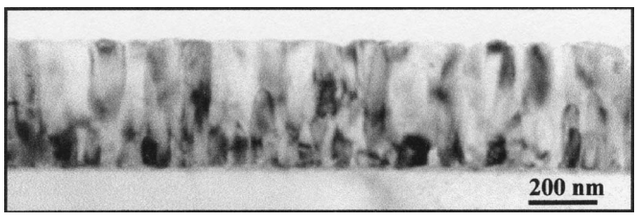

Figure 1. Cross section TEM micrograph of an Al-2% atom Cu model alloy.

Microstructural stability.— TEM examinations were performed on specimens immediately after synthesis and after aging at room temperature for times up to 34 days.

Electrochemical measurements.— Electrochemical studies were performed at 293 K on the freshly deposited and naturally aged alloys. A 0.1 M Na_2SO_4-containing electrolyte, prepared by dissolving the salt in distilled water, was employed; all chemicals were of analytical reagent grade. The sample area exposed to the solution in contact with air was 1 cm^2; no surface preparation was performed on the specimens before electrochemical study. A three-electrode electrochemical cell was used, including a large-surface-area platinum grid as the auxiliary electrode and a saturated calomel reference electrode (SCE). Open-circuit potential (OCP) values were recorded during immersion in the electrolyte for 1 h, corresponding to the time necessary for stabilization. Potentiodynamic polarization curves were also obtained by scanning the potential from the OCP toward the anodic or cathodic direction at a rate of 1 V/h. All potentials are relative to the SCE.

Results and Discussion

Alloy characterization.— A TEM micrograph of a cross section of the Al-2 atom % Cu alloy, revealing an alloy film of uniform thickness, is shown in Fig. 1. Generally, for all the alloys, uniform films were evident with no porosity and good adhesion to the substrate. For the Al-2 atom % Cu alloy, columnar grains are evident that traverse the film thickness. For EDS analysis, 10 measurements were performed for each film by scanning the alloy layer perpendicular to the alloy layer/substrate interface. Further, for each alloy, the procedure was repeated five times by moving the beam 300 nm along an axis parallel to the alloy layer/substrate interface. A beam of nominal diameter of 7 nm was used to optimize spatial resolution and count rate. Figure 2 shows EDS results for alloys of copper contents between 0 and 40 atom %; only 10 measurements are given for an alloy, corresponding to a line scan perpendicular to the alloy layer/substrate interface (Fig. 2a). The mean copper content can be compared with the copper content estimated from consideration of the sputtering conditions, with Fig. 2b giving the standard deviation of the measurements for each alloy. The difference between the measured mean copper content and the estimated value is relatively low, confirming the good control of composition offered by magnetron sputtering (Fig. 2a). Figure 2b reveals that the measurements are reproducible for copper contents below 7 atom %; for increased copper contents, the standard deviation values are higher except for the Al-33 atom % Cu alloy, of composition corresponding to the θ phase.

Concerning EELS probing, quantitative analysis was performed for the Cu $L_{2,3}$-edge and the Al K-edge in the spectra, providing similar information to that from EDS. Further, from comparison of the ELNES profiles with reference specimens of metallic copper and selected copper oxides, it is concluded that copper is in the metal form in the film, as expected (Fig. 3).

Figure 4 gives typical cross-sectional micrographs of the alloys with copper contents between 0 and 100 atom %, revealing the grain size dependency on copper content. For relatively pure aluminum, columnar grains traversing the film thickness are displayed. For alloys of copper content up to 5 atom %, the grain morphology was similar. For the Al-7 atom % Cu alloy, the microstructure was finer, with both columnar grains and fine equiaxed grains present. The fine

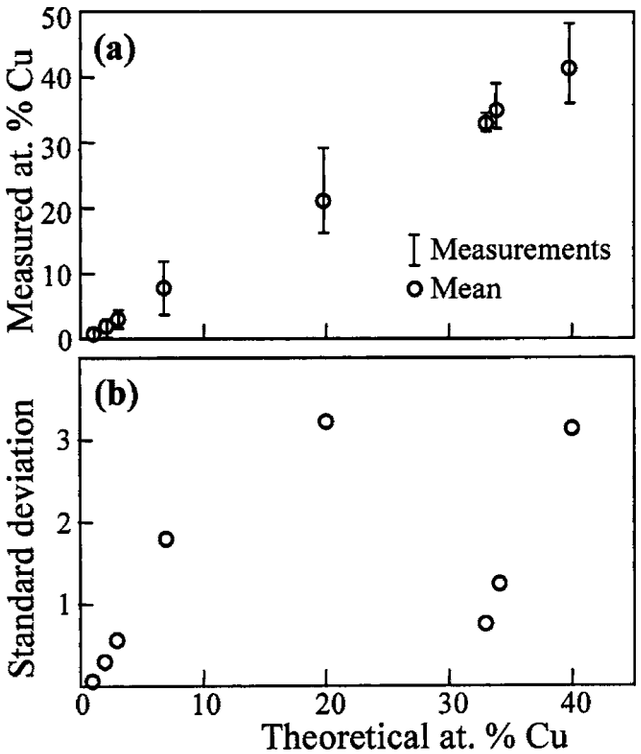

Figure 2. EDS analysis of the Al-Cu thin films: (a) measured copper content and mean copper content and (b) standard deviation on the copper content calculated on the basis of 10 measurements as a function of the predicted copper content in the thin film.

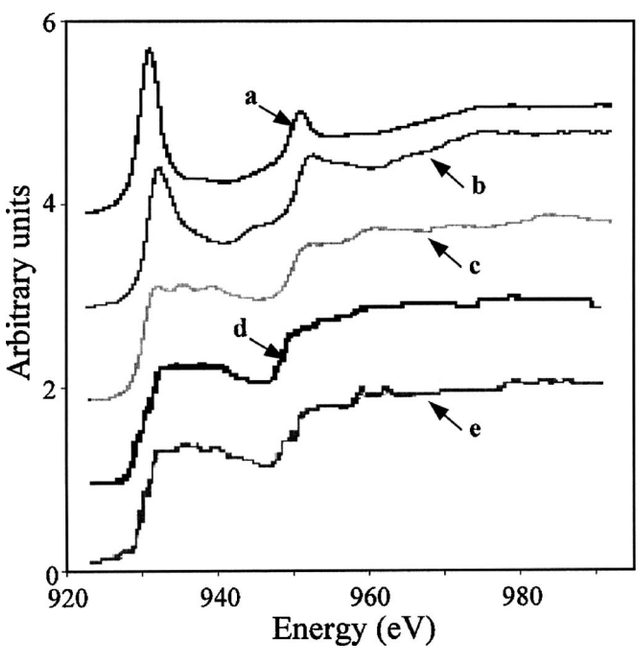

Figure 3. ELNES profiles of the Cu L_{23}-edge for (a) CuO, (b) Cu_2O, (c) metallic copper, (d) Al-22 atom % Cu, and (e) Al-33 atom % Cu. (a), (b), and (c) are reference samples.

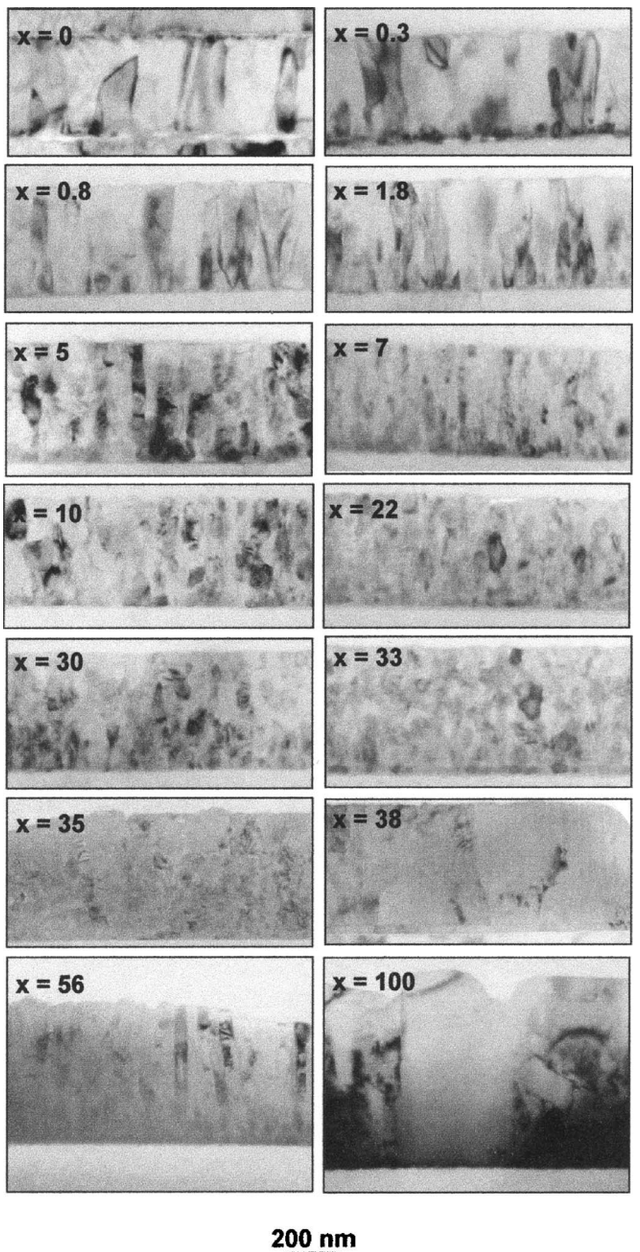

Figure 4. TEM micrograph of an Al-*x* atom % Cu alloy.

grains were in line with an axis perpendicular to the alloy layer/substrate interface. For copper contents between 10 and 33 atom %, only fine equiaxed grains were revealed. With further increase of copper content, columnar grains were again observed and, at 38 atom % copper, the microstructure displayed only columnar grains across the film thickness.

The results showed a strong influence of copper content on the grain morphology. The Al-33 atom % Cu alloy appears to be of a critical composition. This composition corresponds to the stoichiometry of the θ-phase which may suggest a correlation between the copper content, the grain morphology, and the phases present in the thin films. Thus, electron diffraction was performed on the sections to determine the nature of the phases present in the model alloys of different copper contents. For the alloys containing only columnar grains, diffraction patterns were determined for several grains by moving the beam from the surface to the alloy layer/substrate interface. For the alloys containing fine equiaxed grains, the beam was centered on an individual grain, with diffraction patterns determined for more than 20 grains. For model multiphased alloys, the volume fraction of each phase in the alloy was estimated from the diffraction patterns, providing a good approximation of the metallurgical states of the appropriate films. Figure 5 shows the equilibrium phase diagram corresponding to room temperature, revealing the presence of eight phases depending on alloy copper content. The solubility of copper in aluminum at room temperature is limited at 0.02 atom %. For increased copper contents, the aluminum solid solution, α-Al, coexists with the θ-Al_2Cu phase. Other copper-rich phases can exist such as η_2-AlCu, ξ_2-Al_9Cu_{12}, δ-$Al_{20}Cu_{30}$, γ_2-Al_4Cu_9, α_2 and the copper solid solution, α-Cu. From the literature, some metallurgical phases have been studied widely, whereas little information is available for others.[15,16] Therefore, here α-Al, θ-Al_2Cu, η_2-AlCu, ξ_2-Al_9Cu_{12}, δ-$Al_{20}Cu_{30}$, and α-Cu are considered, with relevant crystallographic characteristics given in Table I. Electron diffraction performed in this study on all the model alloys detected only three phases among all the described phases, with Fig. 6 showing the diffraction patterns from these phases, i.e., the α-Al, θ-Al_2Cu, and η_2-AlCu phases. The volume fraction of each of the phases in a particular alloy is estimated in Fig. 7, with the volume fraction suggested from the equilibrium diagram [taking into account the density of each phase (Table I)] also displayed. For the Al-22 atom % Cu, Al-35 atom % Cu, and Al-42 atom % Cu alloys, the results are very similar to those calculated from the equilibrium phase diagram. For the Al-22 atom % Cu alloy, two metallurgical phases, α-Al and θ-Al_2Cu, are evident, with θ being the major phase. For Al-35 atom % Cu and Al-42 atom % Cu alloys, α-Al is not detected according to the equilibrium phase diagram, while θ and η_2 are detected; the volume fraction of η_2 increases from 10 to 50% with increase of

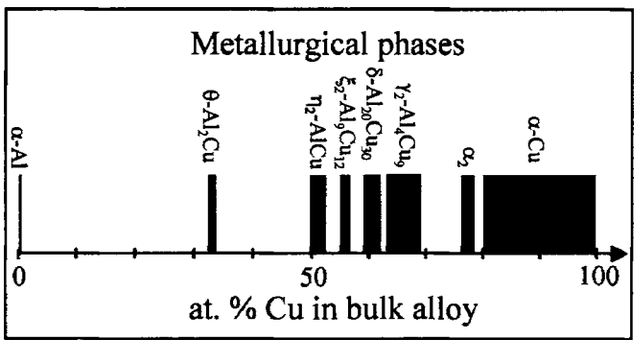

Figure 5. Part of the equilibrium phase diagram at room temperature.

Table I. Crystallographic characteristics of different copper-aluminum phases (JCPDS files).

Phases	Crystallographic cells	Crystallographic parameters	Density (g cm^{-3})
α-Al	FCC	a = 0.4041 nm	2.70
θ-Al_2Cu	Tetragonal	a = 0.604 nm c = 0.486 nm	4.33
η_2-AlCu		a = 0.695 nm	
	C Orthorombic	b = 0.416 nm	
		c = 1.004 nm	4.46
	NaCl Cubic	a = 0.5013 nm	
	CC	a = 0.291 nm	
ξ_2-Al_9Cu_{12}	Monoclinic	a = 0.707 nm b = 0.408 nm c = 1.002 nm	
δ-$Al_{20}Cu_{30}$	Monoclinic		
α-Cu	FCC	a = 0.361 nm	

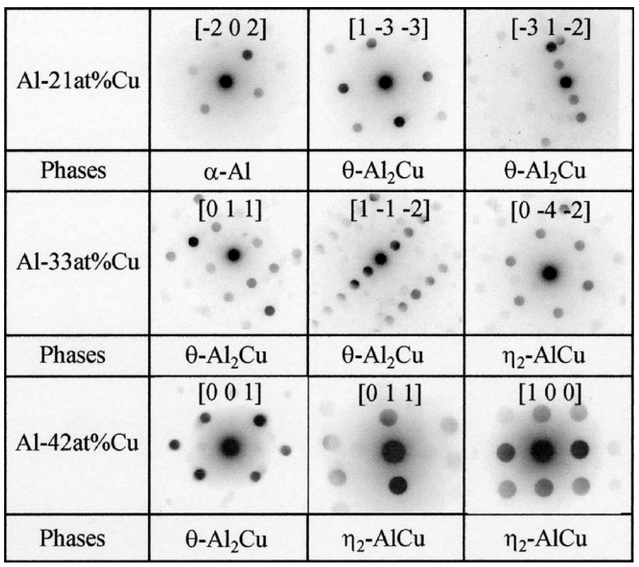

Figure 6. Electron diffraction patterns from the α, θ, and η_2 phases present in the Al–Cu alloys. Examples are given for Al-21 atom % Cu, Al-33 atom % Cu, and Al-42 atom % Cu alloys.

copper content from 35 to 42 atom %. For the Al-33 atom % Cu alloy, the major phase detected is θ phase, while some η_2 phase is evident. This is suggested from the equilibrium diagram, with this composition. For the Al-7 atom % Cu alloy, only α-Al is detected, although from the equilibrium diagram, a multiphased material with θ of volume fraction of 19.4% is estimated. It is possible that the θ precipitates are too small to be detected or the alloy did not correspond to equilibrium conditions due to relatively rapid deposition of material. For the Al-2.5 atom % Cu alloy, only α was also detected, as expected.

Correlation between the copper content, the phases, and the grain size.— Previous characterization of model alloys has shown the presence of two phases, depending on copper content. Further EDS analyses performed on Al-7 atom % Cu, Al-22 atom % Cu, Al-35 atom % Cu, and Al-42 atom % Cu alloys revealed a lack of reproducibility, whereas for the Al-33 atom % Cu alloy and for

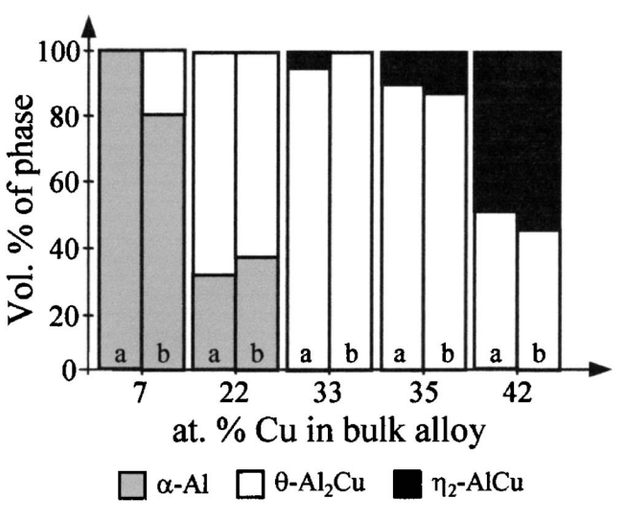

Figure 7. Variation of the volume fraction of the α, θ, and η_2 phases in Al-*x* atom % Cu alloys with copper content (a) experimental values, (b) values determined from the equilibrium phase diagram.

alloys of copper content less than 5 atom %, the standard deviation on the analyses were improved. Alloys of low copper content can be assumed to comprise the α phase only, which may explain the reproducibility. For the Al-7 atom % Cu alloy, the standard deviation on the analyses increased; further, the grain size was different from that observed for α monophased alloys but similar to that of alloys containing both α and θ phases. It was then assumed that Al-7 atom % Cu alloy contained the θ phase, despite the diffraction results. A very small size of θ crystals in this alloy might explain these results. For Al-22 atom % Cu, Al-35 atom % Cu, and Al-42 atom % Cu alloys, the coexistence of two phases (α + θ or θ + η_2) is responsible for the high values of standard deviation; this value decreased for the Al-33 atom % Cu alloy, with its low volume fraction of η_2 phase. Assuming the presence of fine θ crystals in the Al-7 atom % Cu alloy, there was good correlation between EDS analyses and electron diffraction results; both results could also be related to the variation of the grain morphology. Alloys of less than 5 atom % copper were assumed to contain the α phase alone, with only columnar grains observed. When the θ phase precipitates, the grain morphology changes with the formation of fine equiaxed grains which coexist with the columnar grains. The Al-33 atom % Cu alloy, largely comprising the θ phase, revealed only equiaxed grains. For alloys with higher copper contents, the formation of the η_2 phase was related to the presence of new columnar grains. When the volume fraction of the θ phase decreased, the proportion of the surface area covered by equiaxed grains decreased through the evolution of a columnar microstructure.

Previous results showed that it was possible to generate specimens of largely θ-phase as well as α-phase material in alloys of less than 1 atom % copper. Synthesis of alloys containing both θ and η_2 phases was also possible with accurate data on the volume fraction of each phase. These alloys are useful to model, respectively, the corrosion behavior of the aluminum matrix, the θ phase, and that of phases containing very high copper concentration present in industrial alloys. In this work, the results showed that for copper contents up to about 5 atom %, the model alloys comprised the α phase, with little or no θ precipitates; the copper solubility in aluminum at room temperature is 0.02 atom %, indicating the extensive supersaturation of the alloys with copper. Thus, the metallurgical states of the model alloys do not correspond to those predicted from the equilibrium phase diagram. However, specimens comprising α, with a fine precipitation of Guinier-Preston zones, θ″, θ′, and possibly θ (too small a size to be detected) can be used to study the electrochemical behavior of the aluminum matrix containing hardening precipitates. Thus, the thin films allow the electrochemical behavior of the aluminum matrix, the aluminum matrix with hardening precipitates, θ precipitates, and high-copper-content precipitates to be individually studied. The model alloys also enable galvanic coupling tests to be performed, which is of interest in the study of processes proceeding at the interface between two phases. However, it is important to determine the stability of the model alloys during the time between the synthesis and the electrochemical tests.

Metallurgical stability of model alloys.— The metallurgical stability of the model alloys during natural aging at room temperature was examined by studying the microstructure of the alloys after 34 days of aging; TEM observations and EDS analyses were undertaken as well as electrochemical studies. OCP measurements were performed and current-potential curves were generated. The study was focused on the Al-7 atom % Cu alloy, which presented the most significant difference between the predicted and experimentally determined structures. Figure 8 shows the OCP measured after immersion for 1 h in sulfate solution with time of natural aging for the alloy. No variations of more than 10 mV were evident for aging times between 0 and 816 h (34 days). Current-potential curves after different aging times revealed no significant differences. These strongly suggest strongly that natural aging had little or no significant effect on the microstructure of the alloy and hence, the electrochemical behavior of the alloy specimen remained unchanged. TEM

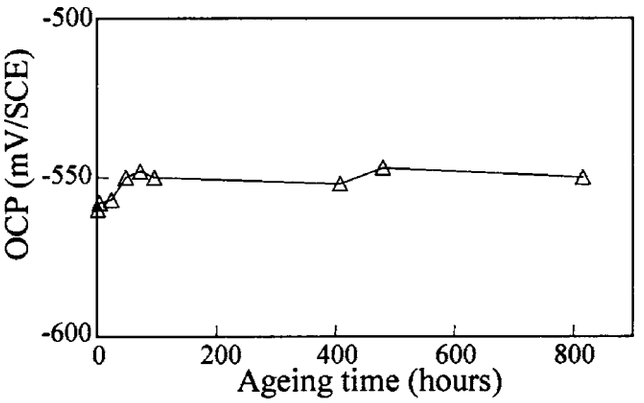

Figure 8. Variation of OCP, measured after 1 h of immersion in 0.1 M Na_2SO_4 solution, with natural aging time at room temperature for an Al-7 atom % Cu alloy thin film.

observations and EDS analyses did not reveal any significant evolution of the microstructure. Further, the results confirmed that model alloys synthesized by magnetron sputtering were metallurgically stable, allowing their electrochemical response to be determined after storage at ambient temperature.

Electrochemical behavior.— Open-circuit potential.— The electrochemical behavior of the model alloys was examined to understand further the influence of copper content on the corrosion behavior of binary Al–Cu alloys. Initially, the variation of the OCP with immersion time in 0.1 M Na_2SO_4 solution was recorded for specimens of copper contents up to 100 atom %. Four different types of behavior were observed and, for clarity, Fig. 9 shows examples of each behavior. The curves obtained for pure aluminum and pure copper are also reported for comparison. For alloys with a low copper content (less than 1.8 atom %), the OCP decreases with increasing immersion time in sulfate solutions, while for alloys with a high copper content (between 35 and 56 atom %), the OCP first increases and then stabilizes at a value similar to that measured for alloys with a very high copper content (70 atom %). For this last type of alloy, the OCP values remained relatively constant with immersion time, with values very close to that measured for pure copper. Finally, alloys with a copper content between 1.8 and 33 atom % (represented by the 22 atom % alloy) present a more complex behavior,

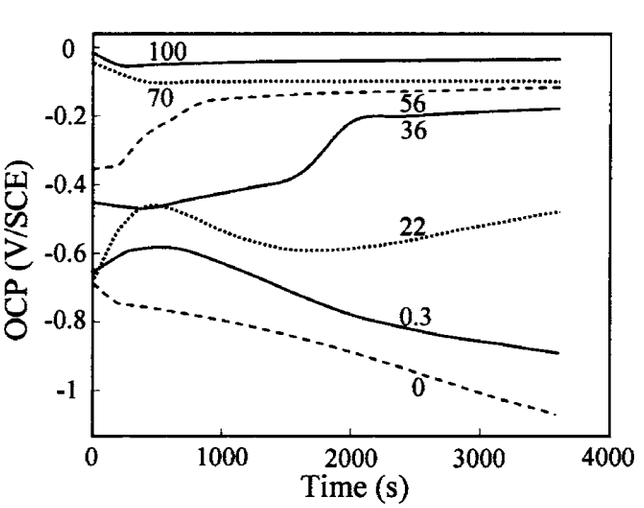

Figure 9. Examples of OCP vs time curves for different Al–Cu alloys in 0.1 M Na_2SO_4 solution (the number near each curve represents the atomic percentage of Cu).

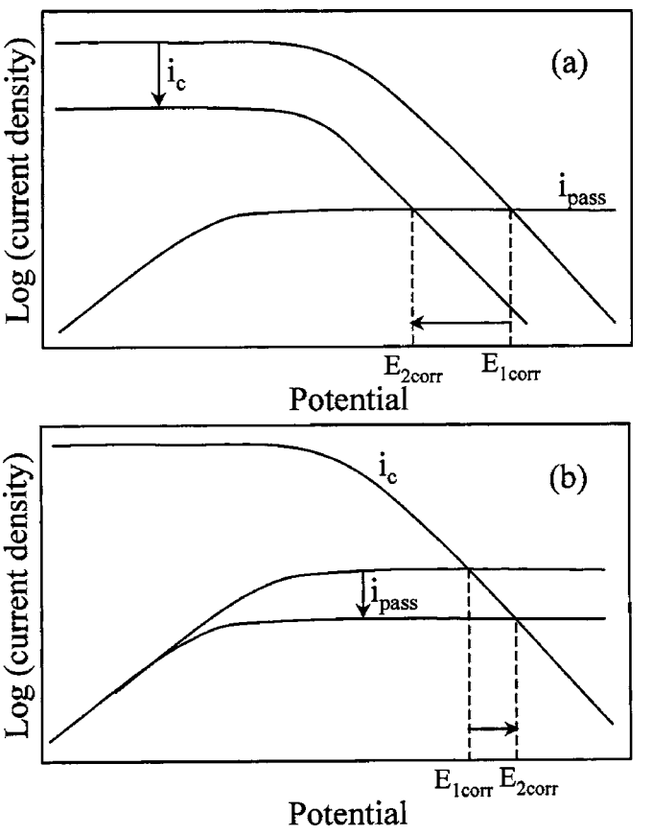

Figure 10. Schematic explanation of the variation of the OCP with time for (a) low-Cu-content and (b) high-Cu-content Al–Cu alloys.

with a nonmonotonous variation of the OCP with time. Figure 10 gives a schematic representation of the current-potential curves obtained for these alloys. For all the alloys, there was no surface preparation before the electrochemical tests. Model alloys were initially covered by an air-formed film which was progressively removed and replaced by a more stable film formed in sulfate solution. For alloys with a low copper content (less than 1.8 atom %), it has been shown, in previous work, that the oxide film was a copper-free alumina film, i.e., a very poorly conductive film.[17] Thus, when model alloys were immersed into sulfate solutions, the growth of this alumina film led to a strong decrease of the oxygen reduction rate while the passive plateau was not really modified. The result was the decrease of the OCP as explained schematically in Fig. 10a. For alloys with a high copper content, there was incorporation of copper into the oxide film which led to a more conductive oxide film.[17] The modification of the oxygen reduction rate was then negligible in comparison with the decrease of the passive current, leading to an increase of the OCP with oxide film growth as shown in Fig. 10b. For model alloys of an intermediate copper content, electron diffraction experiments showed that copper-poor phases and copper-rich phases coexist in the materials; the structure of the oxide film may be more complicated, which explained the nonmonotonous variation of the OCP with immersion time.

For all the alloys, the OCP was relatively stable after 1 h of immersion. Figure 11 shows the variation of the OCP measured after 1 h of immersion in sulfate solution with copper content in the thin alloy films; the resultant curves showed two zones with a logarithmic variation of the OCP with copper content. The transition between these two zones corresponded to a 33 atom % copper content, i.e., a θ-monophased alloy. In the first part of the curve, the OCP strongly increased over a narrow copper range (a few hundreds of millivolts for a copper content variation of only a few atom %), and

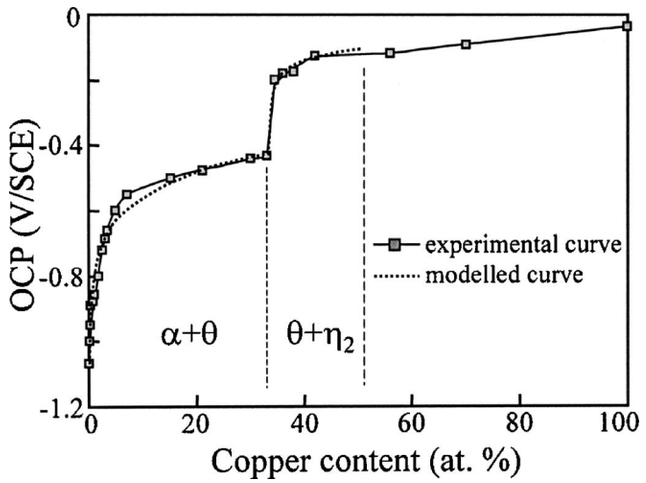

Figure 11. Influence of the copper content on the OCP of Al–Cu alloys after 1 h of immersion in 0.1 M Na_2SO_4 solution.

then slowly increased over a wider copper range (about 100 mV for a copper content variation of 25 atom %), even though the proportion of θ phase significantly increased. In the second part of the curve (copper content 33–50 atom %), a fast increase of OCP over a narrow copper content range was followed by a slow increase of the OCP to that of pure copper. For alloys with more than 50 atom % Cu, there was no significant variation of the OCP. The variation of OCP with copper content can be explained by comparing the potentiokinetic polarization curves of the different alloys.

Current-potential curves.— Figure 12 presents the current-potential curves recorded in 0.1 M Na_2SO_4 solution for specimens of copper contents from 0 to 100 atom %. Results were obtained for 23 different copper contents, but here, for clarity, two figures are presented which correspond to 10 copper contents. These results are sufficient to propose an accurate explanation. The results showed that except for alloys of very high copper content (≥70 atom % Cu), the anodic part of the current-potential curves presented a well-defined passivity plateau above the corrosion potential, with a passive current density varying in a narrow range (from 10^{-6} to 3×10^{-6} A cm^{-2}). The results thus revealed that both the α-Al, θ, and η_2 phases passivated in sulfate solution. Further, at high potentials, for alloys of copper content above 1.8 atom % Cu, pitting was evident in the curves, with a current increase at sufficiently high potential. This can be explained by the aggressivity of sulfate ions to copper; it is known that sulfate ions lead to pit growth on pure copper.[19] Then it was observed that alloys of very high copper content, i.e., alloys with more than 70 atom % Cu, reveal a high anodic current density (10^{-5} A cm^{-2}) without a passivity plateau after the corrosion potential. For pure copper also, no passivity plateau was observed because the corrosion potential corresponded to a pitting potential. These results showed that in sulfate solutions, α-phase alloys remained passive over the entire anodic domain, with sulfate ions regarded as inhibitive species toward pure aluminum. Conversely, alloys with copper-rich phases (θ and η_2 phases) underwent pitting. These results showed that it was interesting to study the electrochemical behavior of binary Al–Cu alloys in sulfate solutions because these species, which are considered as inhibitive species for pure aluminum, promoted pitting on Al–Cu alloys of sufficiently high copper content. This can be related to the reactivity of copper-rich intermetallics present in 2XXX aluminum alloys when immersed in sulfate solutions.[1] The anodic currents associated with pitting in Fig. 12 were not very high, because when a pit formed on an Al–Cu alloy which corresponded to a 500 nm thick film, it grew through the film and then repassivated when it reached the pure aluminum substrate. In the cathodic domain, significant differences were also observed

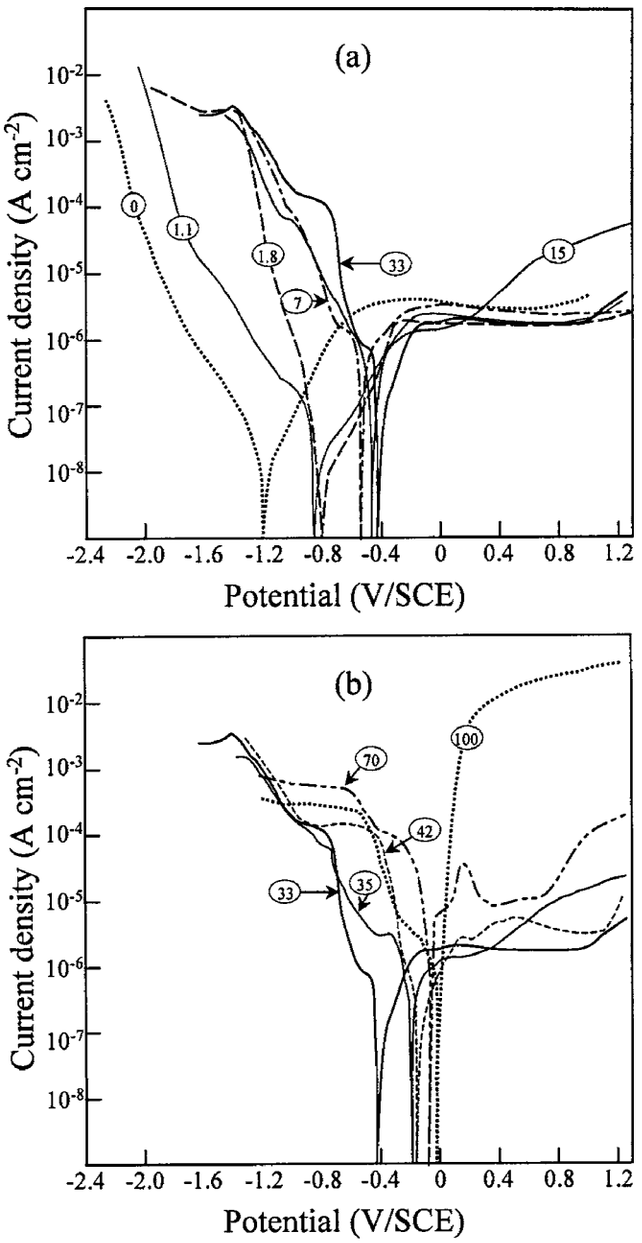

Figure 12. Examples of potential-current curves obtained in a 0.1 M Na_2SO_4 solution for Al–Cu alloys containing (a) from 0 to 33 atom % Cu and (b) from 33 to 100 atom % Cu.

with the copper content of the alloys. Alloys containing up to 1.1 atom % Cu, i.e., α-phase alloys, showed cathodic behavior similar to that of relatively pure aluminum, with a very low cathodic current density. This can be correlated with the results shown in Fig. 9. The growth of a copper-free alumina film, i.e., a poorly conductive film on these low-copper alloys, explained the low cathodic current density. Conversely, for alloys containing increased copper, the cathodic current densities were increased. For alloys with a copper content between 1.8 and 33 atom %, the cathodic reaction rate, in particular that of the water reduction, was higher. For alloys with a higher copper content (from 35 atom %), the presence of the η_2 phase (or that of other copper-rich phases) led to the presence of a cathodic plateau corresponding to the limiting current for the oxygen reduction. These results showed that copper-rich phases, i.e., θ and η_2 phases, promoted the cathodic reduction of water and oxygen and

confirmed previously reported observations:[18] for example, it was shown that the Al_2CuMg phase promoted the cathodic reduction of oxygen and significantly influenced the corrosion behavior of AA2024 aluminum alloy. The results presented here also show that the corrosion behavior of the alloys with different copper contents differed mainly in the cathodic region of the current-potential curves, which largely controlled the corrosion potential of the alloys.

Explanation of OCP variations.— Electron diffraction allowed the proportion of each phase to be determined in the model alloys; in particular, Al-33 atom % Cu alloy was found to be θ-monophased. These microstructural analyses allowed the current-potential curves to be modeled in order to explain the variations of the OCP with copper content. Figures 13a and b show the potentiodynamic polarization curves of the α phase (pure Al) and the θ phase (Al-33 atom % Cu); the curves can be explained as the addition of an anodic curve corresponding to the passivity plateau (except for the pitting part at high potential for Al-33 atom % Cu alloy) and a cathodic curve comprised of the oxygen reduction curve with a diffusion plateau at a value of about 2×10^{-6} A cm^{-2} and the water reduction curve. The partial cathodic curve was calculated by assuming a constant anodic current density equal to the passive current for the partial anodic curve. From the schematic partial curves of Fig. 13a and b (dotted curves), it was evident that the oxygen plateaus for the α and θ phases had similar values. However, comparing the activation polarization regions of this reaction, it appeared that at a given potential, the rate of the oxygen reduction was much higher on θ phase than on α phase.

In (α + θ)-containing alloys, i.e., alloys with a copper content in the 0–33 atom % Cu range, the current density i_c of oxygen reduction depended on the volume proportions (S_α and S_θ) according to

$$i_c = S_\alpha i_c(\alpha) + S_\theta i_c(\theta) \quad [1]$$

If the copper content was higher than a few atom %, the current on the α phase was negligible compared with the current on the θ phase, and then

$$i_c = S_\theta i_c(\theta) \quad [2]$$

Further, the cathodic current depended on the potential according to the Tafel equation

$$E = E_0 + b_c \log[i_c/i_c^0] \quad [3]$$

Combining Eq. 2 and 3 gave

$$E = E_0 + b_c \log[S_\theta i_c(\theta)/S_\theta i_c^0(\theta)] \quad [4]$$

The corrosion potential, E_{corr}, was obtained when $S_\theta\ i_c(\theta)$ was equal to the passive current, i_{pass}

$$E_{corr} = E_0 + b_c \log[i_{pass}/S_\theta i_c^0(\theta)] \quad [5]$$

The current density $i_c^0(\theta)$ was a constant, and the passive current could also be considered to be constant because it was nearly similar for all the (α + θ)-containing alloys. Consequently, the corrosion potential was dependent only on the proportion of the θ phase according to the relation

$$E_{corr} = k - b_c \log[S_\theta] \quad [6]$$

Finally, because the proportion of the θ phase varied with the atomic percentage of copper according to the approximate relation

$$S_\theta = 3(\text{atom \% Cu}) \quad [7]$$

the corrosion potential varies logarithmically with the atomic percentage of copper

$$E_{corr} = k - b_c \log[3(\text{atom \% Cu})] \quad [8]$$

Calculations were performed to determine the values of the parameters of Eq. 8, leading to the best fit with the experimental data. A value of −240 mV was obtained for the Tafel slope, which was a plausible value for the oxygen reduction reaction on the θ phase. Figure 11 showed that between 0 and 33 atom % Cu, the experimental values of OCP are close to the values calculated by using Eq. 8 and the previous value of the cathodic Tafel slope (dotted curve).

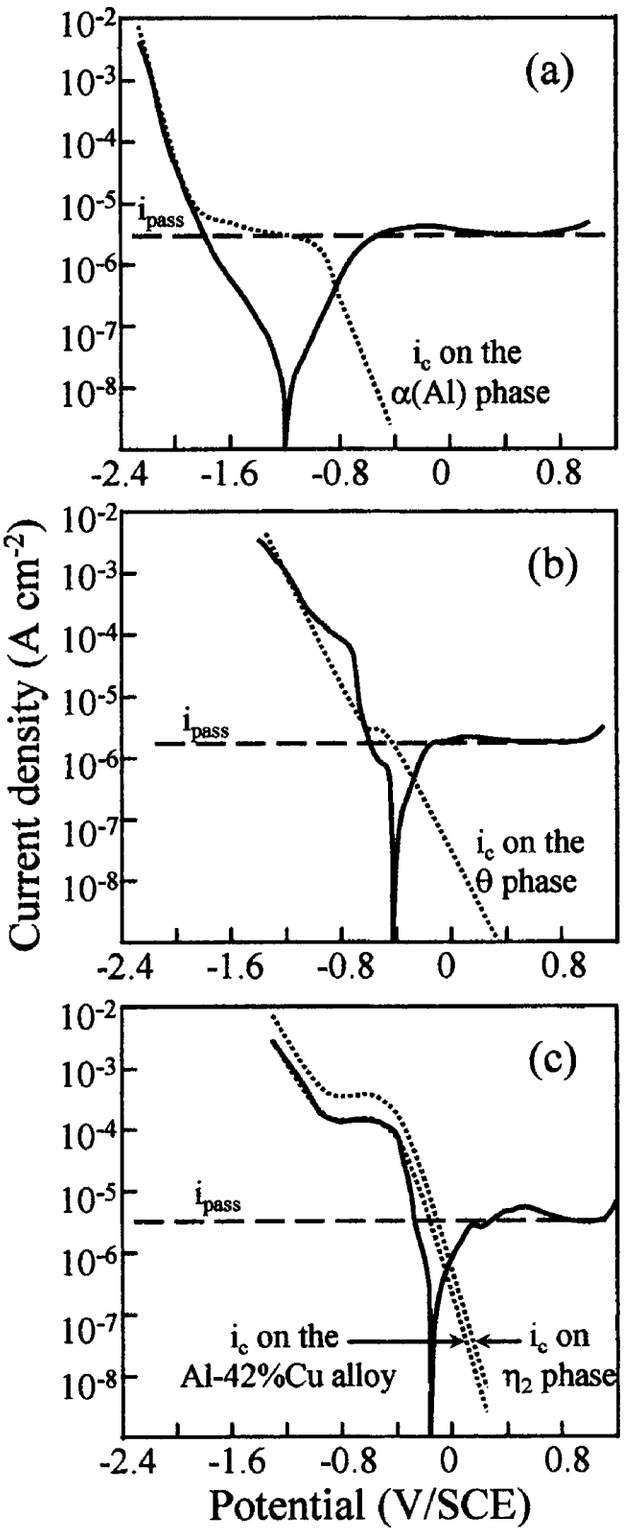

Figure 13. Experimental potential-current curves and partial anodic and cathodic curves for α, θ, and θ + η_2-containing Al–Cu alloys.

Partial curves for the η_2 phase were calculated from the current-potential curves of Al-42 Cu, taking into account the respective

proportion of θ and η_2 phases given by electron diffraction experiments (Fig. 13c). For (θ + η_2)-containing alloys (between 33 and 50 atom % Cu), a logarithmic variation of the OCP with the copper content was also observed in Fig. 11. A similar explanation was also valid for these alloys, because the rate of oxygen reduction on the η_2 phase is much higher than on the θ phase (Fig. 13b and c). In this case, the best fit between the experimental data and the model was obtained with a value of −95 mV for the Tafel slope for the oxygen reduction reaction on η_2 phase. In this case, there is also good agreement between the experimental and the calculated values. For (η_2 + ξ_2) or (ξ_2 + δ)-containing alloys, the previously established behavior was not observed because the OCP increased slightly between 50 and 100 atom % Cu. This observation resulted from the similar rate of oxygen reduction on the highest Cu-containing phases (η_2,ξ_2,δ,γ_2, …) (Fig. 12).

The results thus showed that for alloys containing both α and θ phases, the corrosion behavior was controlled by the θ phase even when the θ volume fraction was low. This result is in agreement with previously published work,[18] which showed that the corrosion potential of AA2024 alloy was controlled by Al_2CuMg particles even though the surface coverage was only about 4% of the total surface area. For alloys of copper contents from 33 to 35 atom %, the sudden increase in OCP was related to the presence of the η_2 phase. The presence of a low fraction of η_2 phase was also sufficient to control the corrosion behavior of alloys containing both θ and η_2 phases. As a conclusion, it was shown that the kinetics of the cathodic reaction increased from α to θ and then to the η_2 phases. In an alloy containing two phases (α and θ phases or θ and η_2 phases), the phase of higher copper content controlled the corrosion potential of the alloy, even though present at low volume fraction.

Further, significant difference between α, θ, and η_2 phases was their susceptibility to pitting (Fig. 12). Observations of the electrodes after completing the anodic polarization behavior showed that, for alloys of low copper content, the surface was little altered (Fig. 14a-c). Conversely, pits were observed for alloys of more than 2 atom % Cu (Fig. 14d-g). This is in agreement with the shape of the anodic part of the current-potential curves. In the anodic domain, the growth of the pits led to a significant increase of the anodic current only at high potentials.

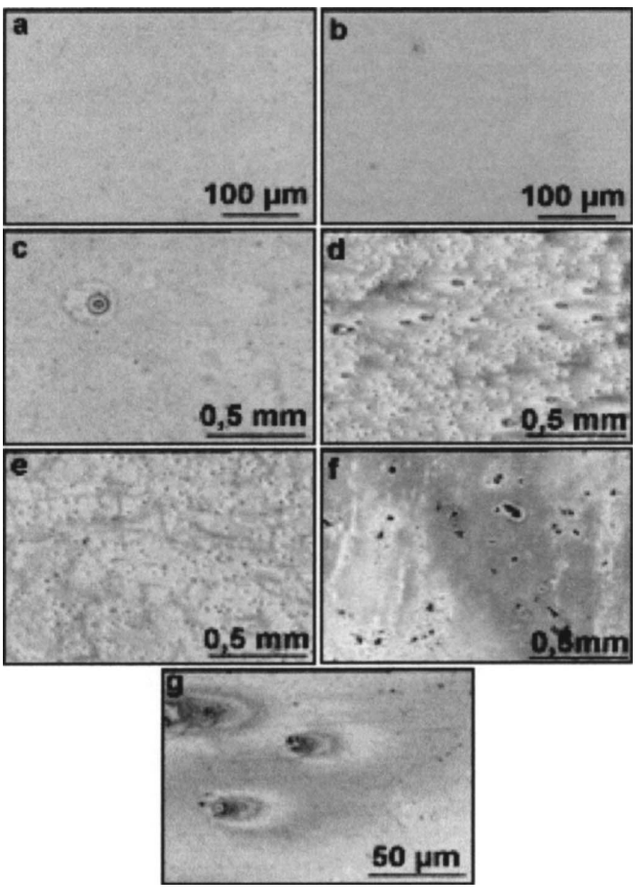

Figure 14. Optical micrographs of Al-*x* atom % Cu after plotting of the anodic potential-current curves in 0.1 M Na_2SO_4 solution: (a) *x* = 0; (b) *x* = 0.3; (c) *x* = 3.5; (d) *x* = 7; (e) *x* = 33; (f) *x* = 70; and (g) *x* = 100.

Conclusions

The corrosion behavior of copper-containing aluminum alloys can be studied by using model alloys, generated by magnetron sputtering, which enables binary Al–Cu alloys to be prepared with controlled chemical composition. Synthesis of α-Al and θ-Al_2Cu monophased alloys was possible, allowing the corrosion behavior of the individual phase to be examined. Depending on the copper content, multiphased materials may also be synthesized: for some multiphase alloys (of copper content between 5 and about 15 atom %), the volume fractions of the phases did not correspond precisely to those given by the equilibrium phase diagram, but the results showed that the model alloys were stable at room temperature. Electrochemical responses showed that the corrosion behavior of α, θ, and η_2 phases differed strongly in the cathodic region. Further, in the anodic region, phases with high copper content were found to suffer pitting in sulfate solutions while the α phase remained passive.

Centre National de la Recherche Scientifique assisted in meeting the publication costs of this article.

References

1. C. Blanc, B. Lavelle, and G. Mankowski, *Corros. Sci.*, **39**, 495 (1997).
2. C. Blanc, S. Gastaud, and G. Mankowski, *J. Electrochem. Soc.*, **150**, B396 (2003).
3. R. G. Buchheit, R. P. Grant, P. F. Hlava, B. McKenzie, and G. L. Zender, *J. Electrochem. Soc.*, **144**, 2621 (1997).
4. A. Conde and J. D. Damborenea, *Corros. Sci.*, **39**, 295 (1997).
5. A. Barbucci, G. Bruzzone, M. Delucchi, M. Panizza, and G. Cerisola, *Intermetallics*, **8**, 305 (2000).
6. P. Schmutz and G. S. Frankel, *J. Electrochem. Soc.*, **145**, 2295 (1998).
7. V. Guillaumin, P. Schmutz, and G. S. Frankel, in *Localized In-Situ Methods for Investigating Electrochemical Interfaces*, A. C. Hillier, M. Seo, and S. R. Taylor, Editors, PV 99-28, p. 339, The Electrochemical Society Proceedings Series, Pennington, NJ (2000).
8. P. Campestrini, E. P. M. Van Westing, and J. H. W. de Wit, in *Proceedings of the 7th International Symposium on Electrochemical Methods in Corrosion Research*, on CD ROM, Paper 152 (2000).
9. R. G. Buccheit, M. A. Martinez, and L. P. Montes, *J. Electrochem. Soc.*, **147**, 119 (2000).
10. Th. Suter and R. C. Alkire, *J. Electrochem. Soc.*, **148**, B36 (2001).
11. M. Shao, Y. Fu, R. Hu, and C. Lin, *Mater. Sci. Eng., A*, **344**, 323 (2003).
12. M. A. Paez, O. Bustos, G. E. Thompson, P. Skeldon, K. Shimizu, and G. C. Wood, *J. Electrochem. Soc.*, **147**, 1015 (2000).
13. Y. Liu, E. A. Sultan, E. V. Koroleva, P. Skeldon, G. E. Thompson, X. Zhou, K. Shimizu, and H. Habazaki, *Corros. Sci.*, **45**, 789 (2003).
14. S. Garcia-Vergara, P. Skeldon, G. E. Thompson, P. Bailey, T. C. Q. Noakes, H. Habazaki, and K. Shimizu, *Appl. Surf. Sci.*, **205**, 121 (2003).
15. A. J. Bradley, H. J. Goldschmidt, and H. Lipson, *J. Inst. Met.*, **63**, 149 (1938).
16. A. J. Bradley and P. Jones, *J. Inst. Met.*, **51**, 131 (1933).
17. J. Idrac, P. Skeldon, Y. Liu, T. Hashimoto, G. Mankowski, G. Thompson, and C. Blanc, in *The 9th International Symposium on the Passivation of Metals and Semiconductors, and Properties of Thin Oxide Layers*, Ph. Marcus and V. Maurice, Editors, p. 167, Elsevier, New York (2006).
18. C. Blanc, A. Freulon, M. C. Lafont, Y. Kihn, and G. Mankowski, *Corros. Sci.*, **48**, 3838 (2006).
19. J. P. Duthil, G. Mankowski, and A. Giusti, *Corros. Sci.*, **38**, 1839 (1996).